

## Article

# Structural, Thermal, and Electrical Properties of Poly(Ethylene Oxide)—Tetramethyl Succinonitrile Blend for Redox Mediators

Ravindra Kumar Gupta <sup>1,\*</sup> , Hamid Shaikh <sup>2</sup> , Ahamad Imran <sup>1</sup>, Idriss Bedja <sup>3</sup>  
and Abdullah Saleh Aldwayyan <sup>4,5</sup> 

<sup>1</sup> King Abdullah Institute for Nanotechnology, King Saud University, Riyadh 11451, Saudi Arabia

<sup>2</sup> SABIC Polymer Research Center, College of Engineering, King Saud University, Riyadh 11421, Saudi Arabia

<sup>3</sup> Cornea Research Chair, Department of Optometry, College of Applied Medical Sciences, King Saud University, Riyadh 11433, Saudi Arabia

<sup>4</sup> Department of Physics and Astronomy, College of Science, King Saud University, Riyadh 11451, Saudi Arabia

<sup>5</sup> K.A. CARE Energy Research and Innovation Center, King Saud University, Riyadh 11451, Saudi Arabia

\* Correspondence: rgupta@ksu.edu.sa

**Abstract:** An all-solid-state dye-sensitized solar cell is one of the non-fossil fuel-based electrochemical devices for electricity generation in a high-temperature region. This device utilizes a redox mediator, which is a fast ion-conducting solid polymer electrolyte (SPE). The SPE makes the device economical, thinner, and safer in high-temperature regions. The SPE generally has a form of matrix–plasticizer–redox salts. Succinonitrile (SN) is generally employed as a plasticizer for reducing the crystallinity of poly(ethylene oxide), abbreviated as PEO, a common polymeric matrix. In the present paper, the structural and thermal properties of tetramethyl succinonitrile (TMSN) were compared with SN for its application as a solid plasticizer. TMSN and SN both are plastic crystals. TMSN has four methyl groups by replacing the hydrogen of the SN, resulting in higher molecular weight, solid–solid phase transition temperature, and melting temperature. We thoroughly studied the structural, thermal, and electrical properties of the [(1–x)PEO: xTMSN] blend for utilizing it as a matrix, where  $x = 0–0.25$  in mole fraction. The FT-IR spectra and XRD patterns of the blends exhibited PEO-alike up to  $x = 0.15$  mole and TMSN-alike for  $x > 0.15$  mole. Differential scanning calorimetry revealed formation of a eutectic phase from  $x = 0.1$  mole and phase separation from  $x = 0.15$  mole. The blends with  $x = 0.1–0.15$  mole had a low value of PEO crystallinity. Thermogravimetric analysis showed thermal stability of the blends up to 75 °C. The blends exhibited electrical conductivity,  $\sigma_{25^\circ\text{C}}$  more than  $10^{-9}$  S cm<sup>-1</sup>, and Arrhenius behavior (activation energy, ~0.8 eV) in a temperature region, 25–50 °C.

**Keywords:** dye-sensitized solar cell; tetramethyl succinonitrile; polymer electrolyte; blend; redox mediator



**Citation:** Gupta, R.K.; Shaikh, H.; Imran, A.; Bedja, I.; Aldwayyan, A.S. Structural, Thermal, and Electrical Properties of Poly(Ethylene Oxide)—Tetramethyl Succinonitrile Blend for Redox Mediators. *Polymers* **2022**, *14*, 3728. <https://doi.org/10.3390/polym14183728>

Academic Editor: Bożena Jarzabek

Received: 27 July 2022

Accepted: 4 September 2022

Published: 7 September 2022

**Publisher's Note:** MDPI stays neutral with regard to jurisdictional claims in published maps and institutional affiliations.



**Copyright:** © 2022 by the authors. Licensee MDPI, Basel, Switzerland. This article is an open access article distributed under the terms and conditions of the Creative Commons Attribution (CC BY) license (<https://creativecommons.org/licenses/by/4.0/>).

## 1. Introduction

A redox mediator is an integral part of the dye-sensitized solar cell (DSSC). The redox mediator, an I<sup>-</sup>/I<sub>3</sub><sup>-</sup> redox-couple-based electrolyte, regenerates dye via oxidation of iodide at the working electrode. The iodide is regenerated at the counter electrode. The electrolyte also inhibits back electron transfer reactions. In particular, the energy level alignment between the redox level and the ground state of the dye is crucial for charge transfer and dye regeneration. For a review on DSSC, see references [1–5]. An electrolyte can be in a form of liquid, gel, or solid. In the liquid state, an electrolyte has a form of MI–I<sub>2</sub>–solvent, where M is an alkali metal or organic cation. The solvent can be a polar aprotic liquid, an ionic liquid, or both. The liquid nature offers easy preparation of the electrolyte, a high electrical conductivity ( $\sigma_{25^\circ\text{C}} \sim 10^{-2}$  S cm<sup>-1</sup>), a high triiodide apparent diffusion coefficient ( $\sim 10^{-6}$  cm<sup>2</sup> s<sup>-1</sup>), and good interfacial contacts with electrodes [1–5]. This has resulted in solar cell conversion efficiency ( $\eta$ ) as high as 11.9%@100 mW cm<sup>-2</sup> [6]. The Co<sup>2+</sup>/Co<sup>3+</sup>-based liquid electrolytes exhibited better cell performance, such as 13% for SM315 dye [7],

13.6% for ZL003 dye [8], and ~14.3% for ADEKA-1+LEG4 dyes [9]. The  $\text{Cu}^+/\text{Cu}^{2+}$  redox mediators had  $\eta$  ~12.7% for R7+Y123 dyes and 13.1% for Y123+XY1 dyes [10,11]. The liquid nature of the electrolyte, however, enforces hermetic sealing in the DSSC. This is for sustaining the high-pressure build-up because of a large diurnal temperature fluctuation in the Gulf countries, having a long summer with a temperature range of 40–50 °C. This also makes device manufacturing difficult. A gel electrolyte absorbs a large amount of liquid electrolyte in an organic or inorganic framework. This, therefore, possesses the electrical and interfacial properties similar to a liquid electrolyte, and shortcomings as well. A solid electrolyte particularly in a polymeric form is currently of great interest in research work. This eliminates the shortcomings of liquid electrolyte-based DSSC and makes the device lighter, thinner, and safer in high-temperature regions. For a review on electrolytes, see references [12–24].

A solid polymer electrolyte (SPE) in the form of PEO–MI–I<sub>2</sub> is generally used as a solid redox mediator [12–24]. The PEO is an abbreviation of a high molecular weight poly(ethylene oxide), which is an excellent matrix. This is due to its properties such as dielectric constant ( $\epsilon$ ) between 5 and 8 at 25 °C and the Gutmann donor number of 22, resulting in ionic salt dissociation; segmental motion of polymeric chains; ion transportation through its ethereal oxygen; the optimal spacing between coordinating ethereal oxygens for solvation of the lithium ions; a self-standing film formation; ecologically and biologically benign; low material cost; and high thermal stability (~200 °C) [25–28]. The pure PEO-based electrolytes, however, exhibit poor  $\sigma_{25^\circ\text{C}}$ -values ( $\leq 10^{-5}$  S cm<sup>-1</sup>), and thereby,  $\eta < 1\%$  at 1 sun. This was probably due to a higher PEO crystallinity ( $\chi$ ) hindering the ion transport. For decreasing the  $\chi$ -value to nearly zero, thereby increasing the  $\sigma_{25^\circ\text{C}}$ -value more than  $10^{-4}$  S cm<sup>-1</sup>, the PEO was blended with a plasticizer [12–20]. This was a low molecular weight polymer [29–31], ionic liquid [14,32], biopolymer [17], nanoparticle [30,33–36], and plastic crystal [37–40].

Plastic crystals are made of weakly interacting molecules, forming a globular shape due to the orientational or conformational degree of freedom [41]. That is, crystals are either symmetrical around their center or give a sphere by rotation around an axis. The plastic crystal phase exists generally in the cubic form between a solid–solid phase transition temperature ( $T_{\text{PC}}$ ) and melting temperature ( $T_{\text{m}}$ ). Plastic crystals portray a strong diffuse intensity along with the sharp Bragg peaks in the XRD patterns. These also exhibit melting entropy less than 17 J K<sup>-1</sup> mol<sup>-1</sup>, a continuous rise in the value of the dielectric constant on lowering of the temperature, and a wax-like nature. Succinonitrile (SN;  $\text{N}\equiv\text{C}-\text{CH}_2-\text{CH}_2-\text{C}\equiv\text{N}$ ) is a low molecular weight ( $M_{\text{W}} = 80.09$  g mol<sup>-1</sup>) plastic crystal, which possesses a body-centered cubic structure. The plastic crystal phase exists between -38 °C ( $T_{\text{PC}}$ ) and 58 °C ( $T_{\text{m}}$ ). This has two molecules in the unit cell in which the diagonal of the cube possesses the central C–C bond, and the center of the face keeps the N atom [42]. This structure permits the molecular jump. This also has two isomers, gauche and trans. The latter acts as an impurity for creating mono-vacancy in the lattice, resulting in molecular diffusivity. A solid electrolyte, SN–XY, was used for solid–state battery application, where the notations X and Y stand for a cation and an anion of an ionic salt, respectively [43,44]. The succinonitrile showed the solid solvent plasticizing property because of its higher values of molar enthalpy (139.7 kJ mol<sup>-1</sup>), donor number (14 kcal mol<sup>-1</sup>), and  $\epsilon$  (55 at 25 °C and 63 at 58 °C) [43–45]. This also helped in cation transport through its negative partial-charged nitrile group [44]. These properties of the SN forced the blending of PEO and SN in an equal weight proportion [37]. The (PEO–SN) blend had better properties such as a higher  $\sigma_{25^\circ\text{C}}$ -value, a lower  $\chi$ -value, and higher thermal stability along with other beneficial properties of the constituents. Additionally, the (PEO–SN) blend ensued solid redox mediators with better properties, such as  $\sigma_{25^\circ\text{C}} \approx 3\text{--}7 \times 10^{-4}$  S cm<sup>-1</sup>, transparency in visible and IR regions >95%,  $\chi \sim 0\%$ , thermal stability ~125 °C, and  $\eta \approx 2\text{--}3.7\%$  @100 mW cm<sup>-2</sup> with N719 dye [37–40,46].

Recently, Gupta et al. [47] synthesized [(1– $x$ )PEO]<sub>8</sub>:  $x$ TMSN]–LiI–I<sub>2</sub> solid redox mediators, where  $x$  (=0–0.25 mole) is the composition. The abbreviation, TMSN corresponds

to a colorless tetramethyl succinonitrile, which belongs to the plastic crystal family too [41]. As the name implies, the TMSN has four methyl groups by replacing hydrogen atoms of the succinonitrile with a structure,  $\text{N}\equiv\text{C}-(\text{CH}_3)_2\text{C}-\text{C}(\text{CH}_3)_2-\text{C}\equiv\text{N}$ . This has higher values of  $M_W$  ( $136.2 \text{ g mol}^{-1}$ ) and  $T_m$  ( $\sim 171 \text{ }^\circ\text{C}$ ) than those of the succinonitrile [45,48]. The (0.85PEO: 0.15TMSN) blend-based redox mediator achieved  $\sigma_{25^\circ\text{C}}$  of  $1 \times 10^{-4} \text{ S cm}^{-1}$  and pseudo-activation energy ( $B$ ) of  $\approx 0.083 \text{ eV}$ . As indicated by the results of the XRD, differential scanning calorimetry (DSC), and FT-IR spectroscopy, this was due to a decrease in the  $\chi$ -value, which was associated with a large increase in the relative area of  $\omega_{\text{CH}_2}$  mode. This redox mediator attained  $\eta$  of  $\sim 3.5\% @ 100 \text{ mW cm}^{-2}$ , nearly seven times higher than that of the  $\text{PEO}_8\text{-LiI-I}_2$  ( $\eta \sim 0.5\% @ 100 \text{ mW cm}^{-2}$ ). These results motivated us to compare the structural and thermal properties of TMSN with SN and study the effect of TMSN on the structural, thermal, and electrical properties of the [(1-x)PEO: xTMSN] blends, where  $x = 0\text{--}0.25$  mole. These were carried out using FT-IR spectroscopy, XRD, DSC, thermogravimetric analysis (TGA), and impedance spectroscopy. We also included structural, thermal, and electrical properties of the SPE, [0.85 PEO<sub>8</sub>: 0.15 TMSM]–LiI–I<sub>2</sub> for direct comparison [47].

## 2. Materials and Methods

### 2.1. Synthesis

The chemicals PEO ( $M_W \approx 1 \times 10^6 \text{ g mol}^{-1}$ ) and TMSN were procured from Sigma Aldrich, Inc., USA, and TCI, Japan, respectively, and used without purification. The conventional solution cast method was employed for obtaining a self-standing film of the PEO–TMSN blend, which had the steps of (a) a rigorous stirring of the PEO and TMSN in 20-mL acetonitrile at  $65 \text{ }^\circ\text{C}$  for 48 h, (b) casting of the homogeneous solution on a Teflon Petri dish, (c) drying in a nitrogen gas atmosphere (2-weeks), and (d) drying in a vacuum (1 day). For detail on blend synthesis, please see reference [37].

### 2.2. Characterizations

*FT-IR spectroscopy:* A small amount of SN, TMSN, or PEO was homogeneously mixed with dried potassium bromide powder using an Agate pestle and mortar, followed by pelletizing using a die under  $2 \text{ tons cm}^{-2}$  of pressure. A thin film of the blend on the potassium bromide pellet was prepared following the method of Gupta et al. [37]. We collected the absorbance spectrum of the blend in a range of  $400\text{--}4000 \text{ cm}^{-1}$  (resolution,  $1 \text{ cm}^{-1}$ ) and analyzed using the EZ-OMNIC software (Thermo Scientific Inc., Waltham, MA, USA). We employed a Perkin Elmer, Spectrum 100, FT-IR spectrometer (Waltham, MA, USA) for the measurement.

*XRD:* A circular hole of the sample holder was filled in by the SN, TMSN, PEO, or blend film. The XRD pattern was collected using a Bruker, D2 Phaser, X-ray diffractometer (Karlsruhe, Germany), having the specifications:  $\text{CuK}\alpha$  radiation,  $1.54184 \text{ \AA}$ ; range,  $10\text{--}60^\circ$ ; and step,  $0.06^\circ$ .

*DSC:* A few milligrams of the blend was sealed in an aluminum pan. We employed a Shimadzu, DSC-60A, DSC unit (Kyoto, Japan) for the heat flow measurement of the blend. The heating rate was  $10 \text{ }^\circ\text{C min}^{-1}$ . This was performed under the purging of nitrogen gas.

*TGA:* We measured the weight loss of the blend in the temperature range of  $25\text{--}600 \text{ }^\circ\text{C}$  under the purging of nitrogen gas. This was performed using a Shimadzu, DTG-60H, TGA unit (Kyoto, Japan) with a heating rate of  $10 \text{ }^\circ\text{C min}^{-1}$ .

*Electrical conductivity:* Impedance spectroscopy was utilized for the  $\sigma$  measurement of the film, having a thickness of  $l$  and area of  $A$ . This was carried out using a Palmsens4 impedance analyzer (Houten, the Netherlands) with the experimental conditions, such as stainless steel plates as a blocking electrode,  $20 \text{ mV AC}$  voltage, and a frequency range of  $100 \text{ kHz}$  to  $1 \text{ Hz}$ . The Nyquist curve yielded values of bulk resistance and thereby  $\sigma$  [38].

### 3. Results and Discussion

#### 3.1. Comparison of TMSN with SN

Figure 1 shows the FT-IR spectrum of SN, which has sharp vibrational peaks because of the crystalline nature of molecules. The peak values are similar to that reported earlier by Fengler and Ruoff [49] and, therefore, are assigned accordingly. The vibrational modes were denoted by  $\nu$ ,  $\delta$ ,  $\omega$ ,  $t$ , and  $\rho$ , which correspond to stretching, bending, wagging, twisting, and rocking modes, respectively. Figure 1 also portrayed the spectrum of TMSN. The TMSN possesses the  $\text{CH}_3$  groups by replacing H of the succinonitrile. This is, therefore, similar to that of succinonitrile with an influence of the methyl group, resulting in a redshift in several modes and the crystal field splitting phenomenon because of the doubling of the methyl group [50].

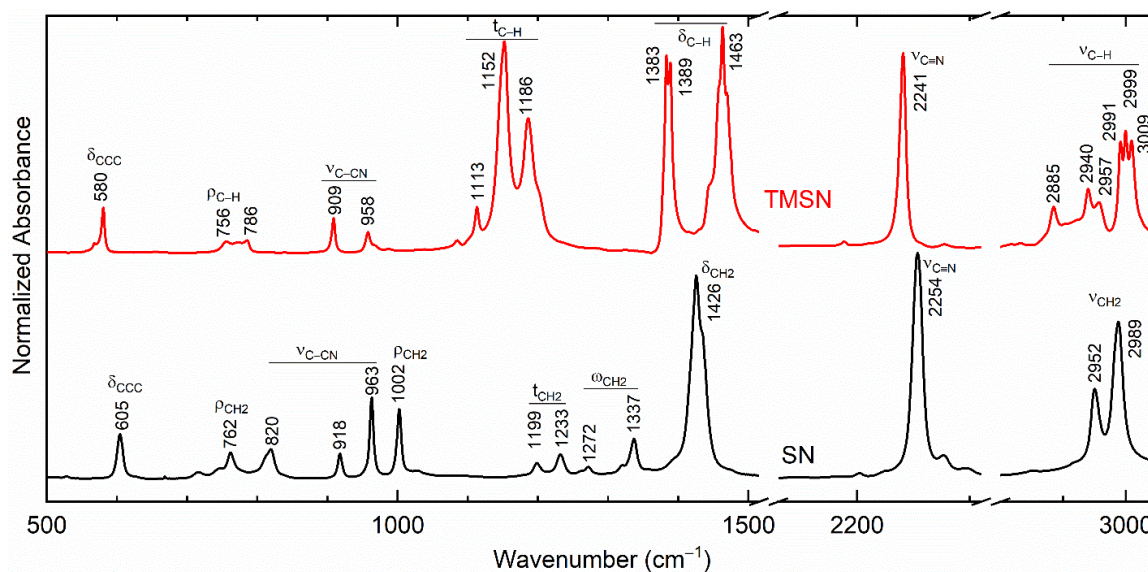


Figure 1. FT-IR spectra of SN and TMSN.

Figure 2 exhibits XRD patterns of SN and TMSN. As mentioned earlier, SN has a bcc structure [42]. This, therefore, portrayed a strong reflection peak at  $\sim 20^\circ$  and a medium peak at  $\sim 28^\circ$  as well as a diffuse peak [37,51]. The replacement of H of the succinonitrile by  $\text{CH}_3$  resulted in TMSN with an XRD pattern having the reflection peaks at  $\sim 12.9$ ,  $14.3$ ,  $15.9$ ,  $17.6$ , and  $29^\circ$ . A thorough Rietveld analysis is, however, required to ascertain its bcc nature.

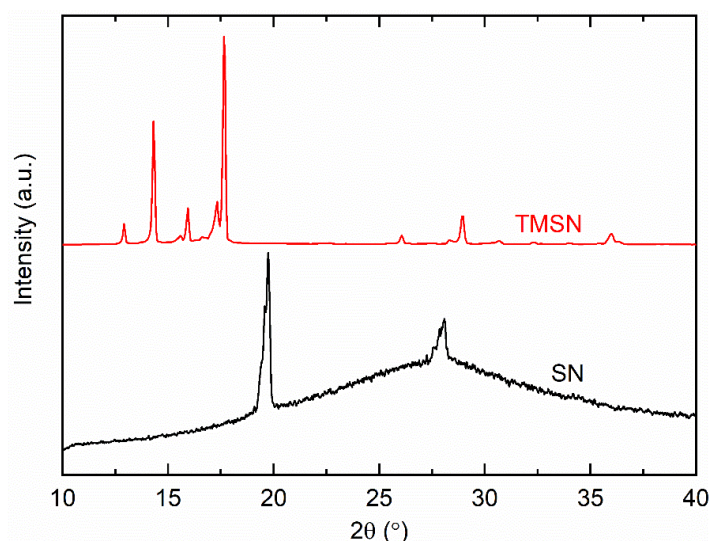


Figure 2. XRD patterns of SN and TMSN.

Figure 3 shows the DSC curves of SN and TMSN. The low molecular weight plastic crystal SN exhibited values of  $T_{PC}$  and  $T_m$  at  $-38$  and  $\sim 58$  °C, respectively, similar to those reported earlier [43,44,51]. The replacement of H of the succinonitrile by  $CH_3$  led to TMSN with a higher molecular weight. This resulted in higher values of  $T_{PC}$  ( $\sim 75$  °C) and  $T_m$  ( $\sim 169$  °C), and was noted to be similar to those reported earlier [45,48].

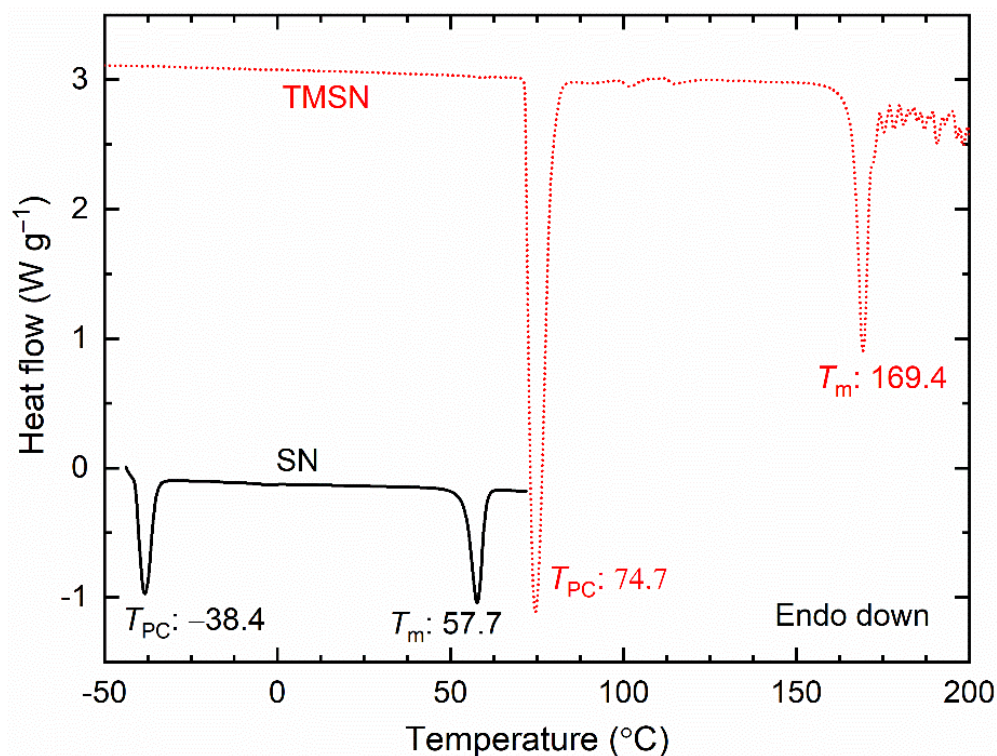
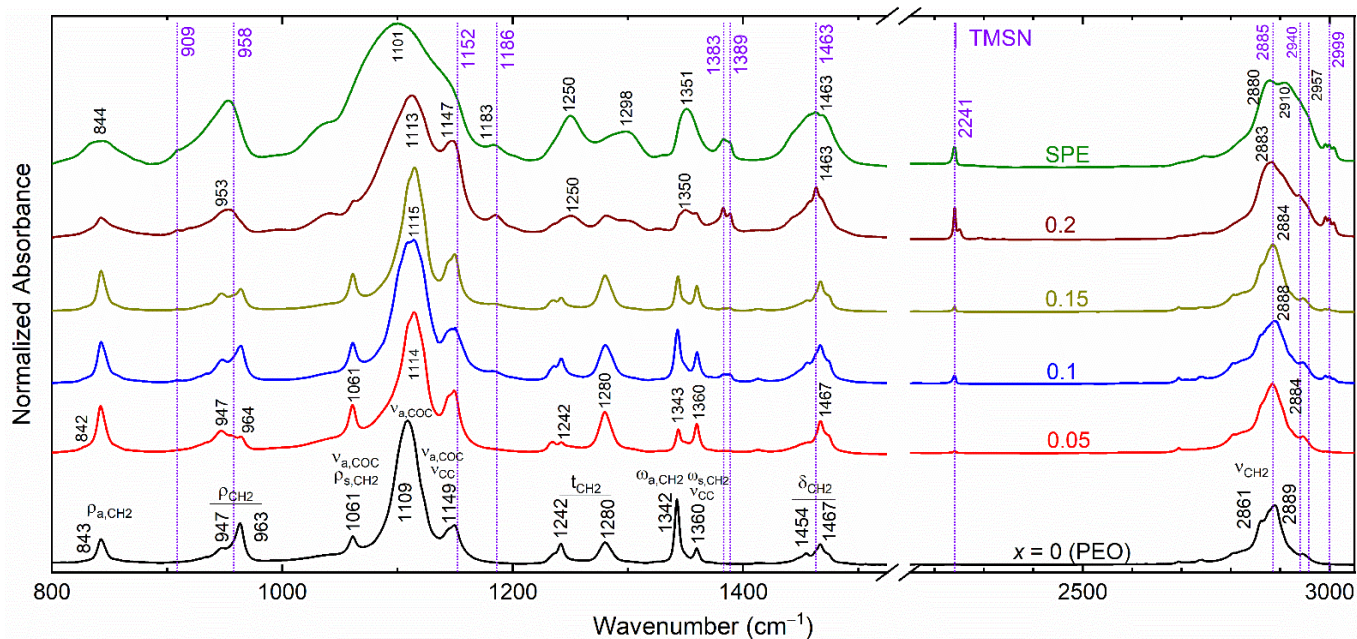


Figure 3. DSC curves of SN and TMSN.

### 3.2. Blend's Characterizations

#### 3.2.1. Structural properties

Figure 4 exhibits FT-IR spectra of the  $[(1-x)PEO: xTMSN]$  blends with  $x = 0-0.2$  mole. The observed modes of TMSN are represented by dotted vertical lines for direct comparison. We included the FT-IR spectrum of the SPE for comparison too. The spectrum of the PEO ( $x = 0$  mole) is similar to that reported earlier by Yoshihara et al. [52]. The peaks are, therefore, assigned accordingly using the conventional notations:  $\nu$  (stretching),  $\delta$  (bending),  $\omega$  (wagging),  $t$  (twisting),  $\rho$  (rocking),  $s$  (symmetric), and  $a$  (asymmetric). The addition of TMSN ( $x = 0.05-0.15$  mole) unaffected the position of several modes of PEO in the figure-print and  $\nu_{C\equiv N}$  regions significantly except for the  $\nu_{a,COC}$  mode at  $\sim 1114$   $cm^{-1}$ . The addition, however, changed the position of the  $\nu_{a,CH_2}$  mode of PEO from  $2889$  to  $2884$   $cm^{-1}$  for the blends with  $x = 0.05$  and  $0.15$  mole. This indicates an increase in the C–H bond of the PEO due to the PEO-TMSN interaction [50]. The addition of  $0.2$  mole, however, significantly changed the position of several modes. For example, the  $\rho_{CH_2}$  modes of PEO at  $947$  and  $963$   $cm^{-1}$  unified at  $953$   $cm^{-1}$ ; the  $\nu_{a,COC}$  mode of PEO shifted to  $1113$   $cm^{-1}$ ; the  $t_{CH_2}$  mode of PEO at  $1242$   $cm^{-1}$  shifted to  $1250$   $cm^{-1}$ ; the  $\omega_{CH_2}$  modes of PEO at  $1342$  and  $1360$   $cm^{-1}$  unified at  $1350$   $cm^{-1}$ ; the  $\delta_{CH_2}$  modes of PEO at  $1454$  and  $1467$   $cm^{-1}$  unified at  $1463$   $cm^{-1}$ ; and the  $\nu_{a,CH_2}$  mode of PEO shifted to  $2883$   $cm^{-1}$ . This also had broadened peaks for the PEO-based modes and quite prominent TMSN-based modes. These demonstrate a significant change in the PEO conformation after  $x = 0.15$  mole [53], as observed by the XRD study, which is discussed later.



**Figure 4.** FT-IR spectra of the [(1- $x$ )PEO:  $x$ TMSN] blends with  $x = 0$ – $0.2$  mole and SPE. The dotted vertical lines correspond to peaks of TMSN.

The SPE, having the blend ( $x = 0.15$  mole) and redox salts, observed a significant change in the PEO structure relative to that of the pure blend. For example, the  $\rho_{\text{CH}_2}$  modes at  $947$  and  $964$   $\text{cm}^{-1}$  unified at  $953$   $\text{cm}^{-1}$ ; the  $\nu_{\text{a,COC}}$  mode at  $1115$   $\text{cm}^{-1}$  shifted to  $1101$   $\text{cm}^{-1}$  along with the merging of the shoulder peaks at  $1061$  and  $1149$   $\text{cm}^{-1}$ ; the  $t_{\text{a,CH}_2}$  mode at  $1242$   $\text{cm}^{-1}$  shifted to  $1250$   $\text{cm}^{-1}$ ; the  $t_{\text{s,CH}_2}$  mode at  $1280$   $\text{cm}^{-1}$  shifted to  $1298$   $\text{cm}^{-1}$ ; the  $\omega_{\text{CH}_2}$  modes at  $1342$  and  $1360$   $\text{cm}^{-1}$  unified at  $1351$   $\text{cm}^{-1}$ ; the  $\delta_{\text{CH}_2}$  modes at  $1454$  and  $1467$   $\text{cm}^{-1}$  unified at  $1463$   $\text{cm}^{-1}$ ; and the  $\nu_{\text{a,CH}_2}$  mode shifted to  $2885$   $\text{cm}^{-1}$ . The PEO bands were noted as quite broad. These observations were similar to those of the blend with  $x = 0.2$  mole, revealing the plasticizing effect of the salt, i.e., the existence of amorphous regions for ion transport [37–39,53]. These changes are due to the salt–PEO–TMSN interactions [37–39].

Figure 5 shows XRD patterns of the [(1- $x$ )PEO:  $x$ TMSN] blends, where  $x = 0$ – $0.25$ , and 1 mole. Having long linear  $-\text{CH}_2-\text{CH}_2-\text{O}-$  chains, the high molecular PEO ( $x = 0$  mole) is semi-crystalline and exhibits strong reflection peaks at  $2\theta$  of  $19.2^\circ$  and  $23.3^\circ$  [37]. The blending of the PEO with TMSN significantly changed the position and intensity of the reflection peaks of both the PEO and TMSN. The change is shown in Table 1 and Figure 6 for direct comparison. The blend with  $x = 0.05$  mole observed a decrease in the  $2\theta$ -value and intensity of PEO, revealing an increase in spacing between polymeric chains and thereby a decrease in PEO crystallinity [40,54]. A further increase in  $x$ -value to  $0.1$  mole led to a slight increase in  $2\theta$ -value, although it still had a low intensity compared to the PEO, indicating restructuring of the PEO chains to accommodate TMSN molecules. The blend with  $x = 0.15$  mole portrayed a peak shift to  $18.3^\circ$  with a lower intensity, revealing a further decrease in PEO crystallinity. This had TMSN peaks at higher  $2\theta$ -values compared to those of the pure TMSN and the TMSN intensities higher than those of the PEO. The blends with  $x = 0.2$  and  $0.25$  mole showed PEO peaks at the  $2\theta$  of  $\sim 18.8^\circ$  and  $\sim 22.9^\circ$  with intensities higher than those of the blend with  $x = 0.15$  mole and lower than those of the pure PEO; however, TMSN peaks became prominent and shifted close to those of the pure TMSN. These indicated recrystallizations of PEO chains and TMSN molecules in the blends, respectively, i.e., the phase separation phenomenon, resulting in an increase in crystallinity of PEO and TMSN for  $x > 0.15$  mole as observed by the DSC study and discussed later. One can also observe that the blends with  $x \leq 0.15$  mole are PEO-alike, and blends with  $x > 0.15$  mole are TMSN-alike. The blends with  $x = 0.1$ – $0.25$  mole also had an additional peak at  $2\theta$  range of  $25.7$ – $26.8^\circ$  apart from a shift in  $2\theta$ -values of PEO and TMSN peaks,

indicating a eutectic phase formation [44]. Figure 5 also shows the XRD pattern of the SPE without the reflection peaks of the PEO, TMSN, LiI, and I<sub>2</sub>. The absence of peaks indicated the formation of the amorphous phase in the SPE, which is due to the salt-PEO-TMSN interactions [37–39]. The DSC revealed a similar result, which is discussed below.

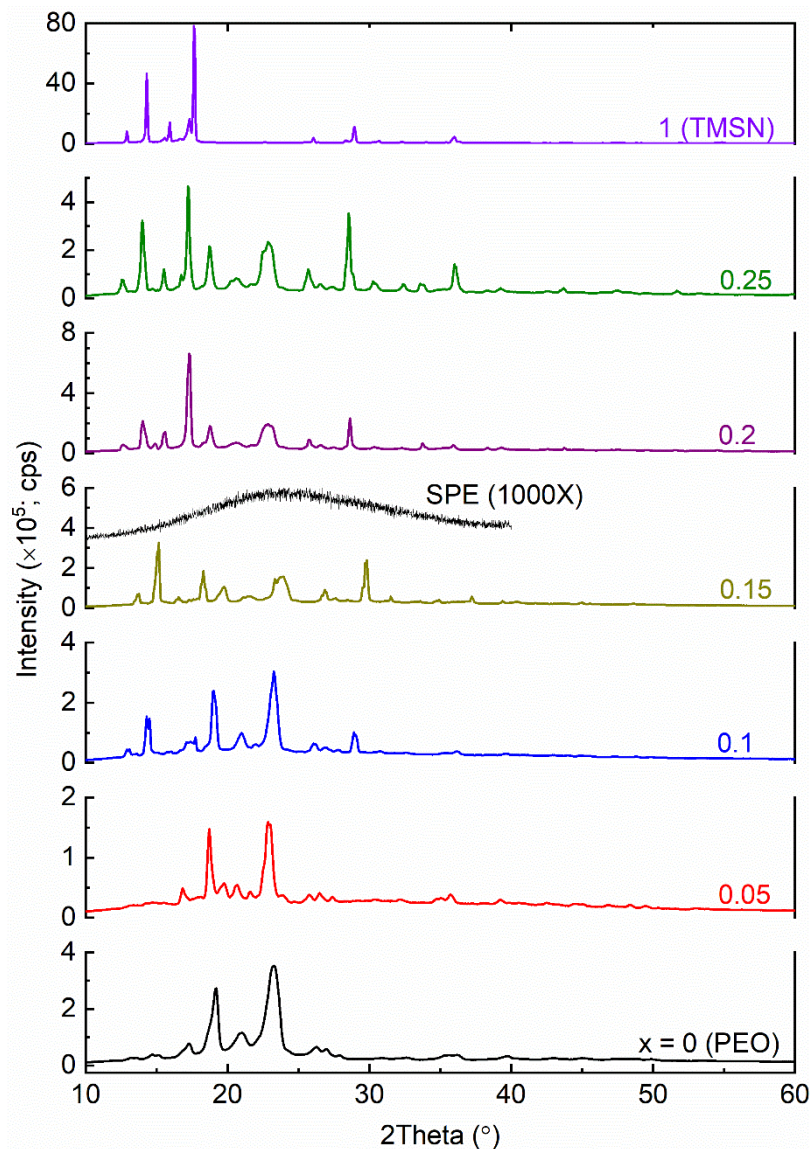
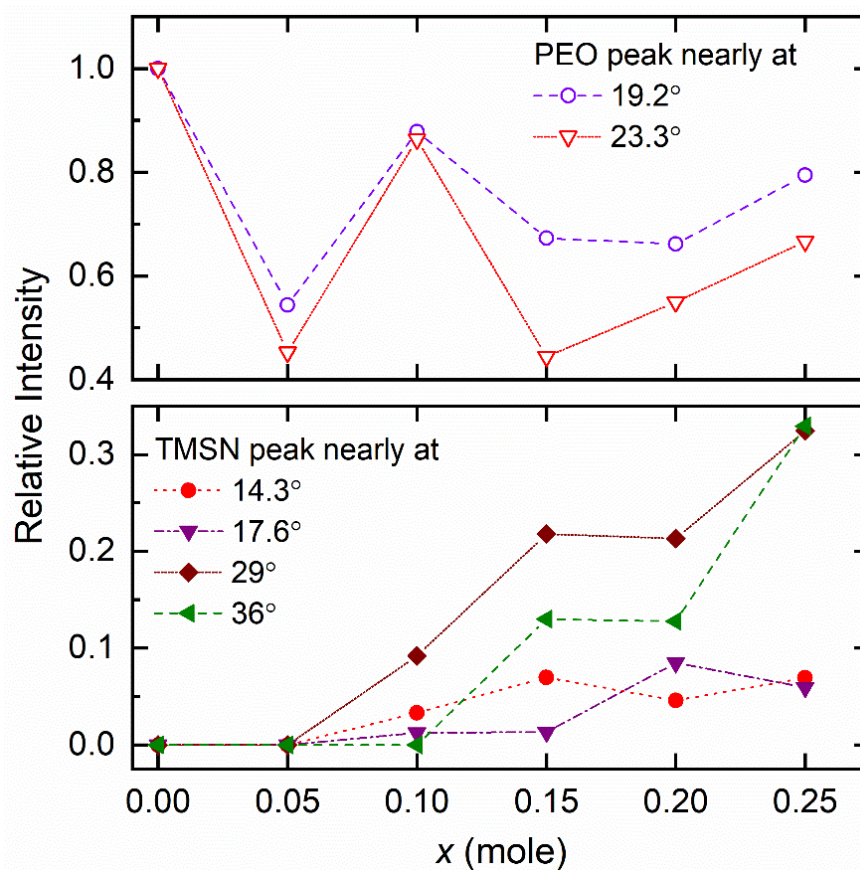


Figure 5. XRD patterns of the [(1-x)PEO: xTMSN] blends (x = 0–0.25, and 1 mole) and SPE.

Table 1. The peak position of ingredients in the XRD patterns of the [(1-x)PEO: xTMSN] blends.

x (Mole)	PEO (°)				TMSN (°)			
	18.7	22.8	28.5	36.0	12.5	14.0	15.5	17.2
0	19.2	23.3	-	-	-	-	-	-
0.05	18.7	22.8	-	-	-	-	-	-
0.1	19	23.3	13.1	14.3	17.5	21.0	28.9	-
0.15	18.3	23.9	13.8	15.2	16.5	19.8	29.8	37.2
0.2	18.8	22.9	12.6	14.0	15.5	17.3	28.6	35.9
0.25	18.7	22.8	12.5	14.0	15.5	17.2	28.5	36.0
1	-	-	12.9	14.3 s <sup>†</sup>	15.9	17.6 vs <sup>†</sup>	29.0	36.0

<sup>†</sup> Notations, s and vs stand for strong and very strong intensity, respectively.



**Figure 6.** Relative intensity of peaks of PEO and TMSN in the [(1-x)PEO: xTMSN] blends, where  $x = 0$ –0.25 mole.

### 3.2.2. Thermal properties

Figure 7 shows the DSC curves of the [(1-x)PEO: xTMSN] blend ( $x = 0$ –0.25, and 1 mole) and SPE. Being a semi-crystalline polymer, the PEO ( $x = 0$  mole) exhibited a strong endothermic peak at 71.5 °C, which is the melting point ( $T_m$ ) of the PEO [37]. The introduction of a small amount of TMSN in PEO ( $x = 0.05$  mole) led to a decrease in the  $T_m$ -value to 62 °C of the blend. A further increase in  $x$  ( $= 0.1$ –0.25 mole) resulted in a secondary endothermic peak ( $T_{ep}$ ) because of the eutectic phase formation [44] along with the  $T_m$ -peak of the blend. The blends with  $x = 0.15$ –0.25 mole were accompanied by a third endothermic peak nearly at 74.5 °C, falling to the domain of the  $T_{PC}$ -peak of the TMSN. We constructed a phase diagram as shown in Figure 8a. This depicted the  $T_m$ -value range between 62 and 66.6 °C with the  $T_{ep}$ -peak at ~60 °C for blends with  $x = 0.1$  and 0.15 mole, 54.6 °C for  $x = 0.2$  mole, and 52 °C for  $x = 0.25$  mole, revealing the eutectic phase formation as observed earlier by the XRD study. The existence of the  $T_{PC}$ -peak for blends with  $x = 0.15$ –0.25 mole indicated the phase separation phenomenon, in which the phase separation is the lowest for the blend with  $x = 0.15$  mole. We estimated the crystallinity ( $\chi$ ) of PEO and TMSN for the blends using an expression,  $\chi = 100 \Delta H/H_{\text{pure}}$ . This has notations,  $\Delta H$  for the heat enthalpy of the blend at  $T_m$  or  $T_{PC}$ , and  $H_{\text{pure}}$  for the heat enthalpy of fully crystalline PEO (193 J g<sup>-1</sup> [37]) or TMSN (134.8 J g<sup>-1</sup>). Figure 8b shows crystallinity of PEO and TMSN for the blends with  $x = 0$ –0.25 mole. The  $\chi$ -value for the PEO decreased sharply up to  $x = 0.1$  mole and then increased relatively slowly and linearly for higher values of  $x$ . The  $\chi$ -value for the TMSN observed a similar trend for the blends with  $x = 0.15$ –0.25 mole. This suggested that the composition,  $x = 0.1$ –0.15 mole, can be utilized as a host matrix for the synthesis of a solid polymer electrolyte. Figure 7 also shows the DSC curve of the SPE for comparison. This portrayed a significant reduction in the heat enthalpy area and existence of the bi-endothermic peaks in the temperature region,

32–40 °C relative to the matrix ( $x = 0.15$  mole). This indicated the eutectic phase formation with a small PEO crystallinity (1.7%) [47]. This curve had no  $T_{PC}$  peak either, revealing the salt–PEO–TMSN interactions [37–39].

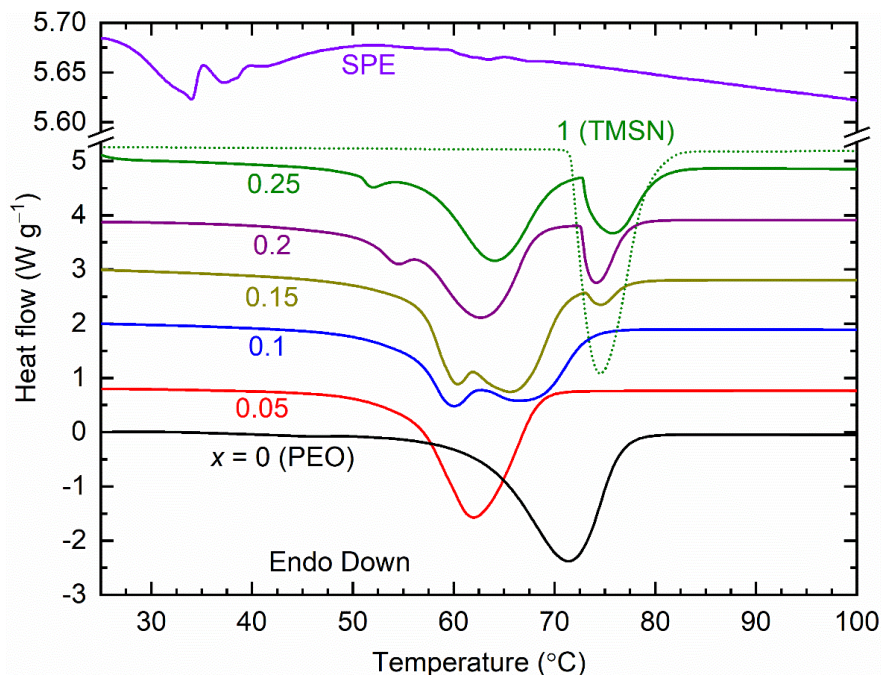


Figure 7. DSC curves of the [(1-x)PEO: xTMSN] blends ( $x = 0-0.25$ , and 1 mole) and SPE.

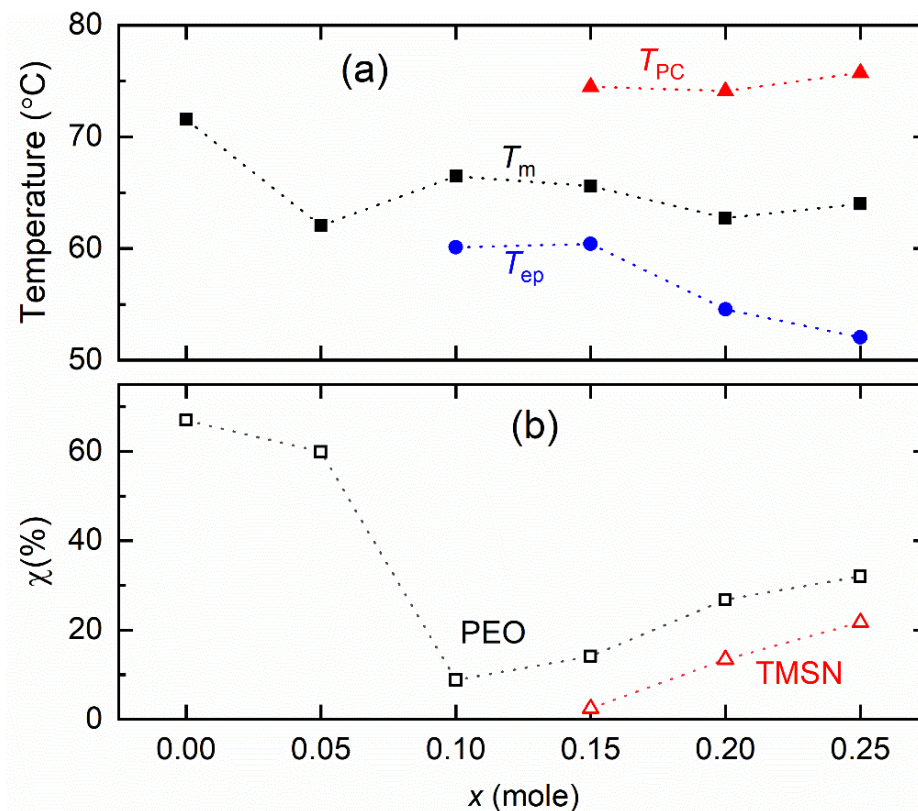
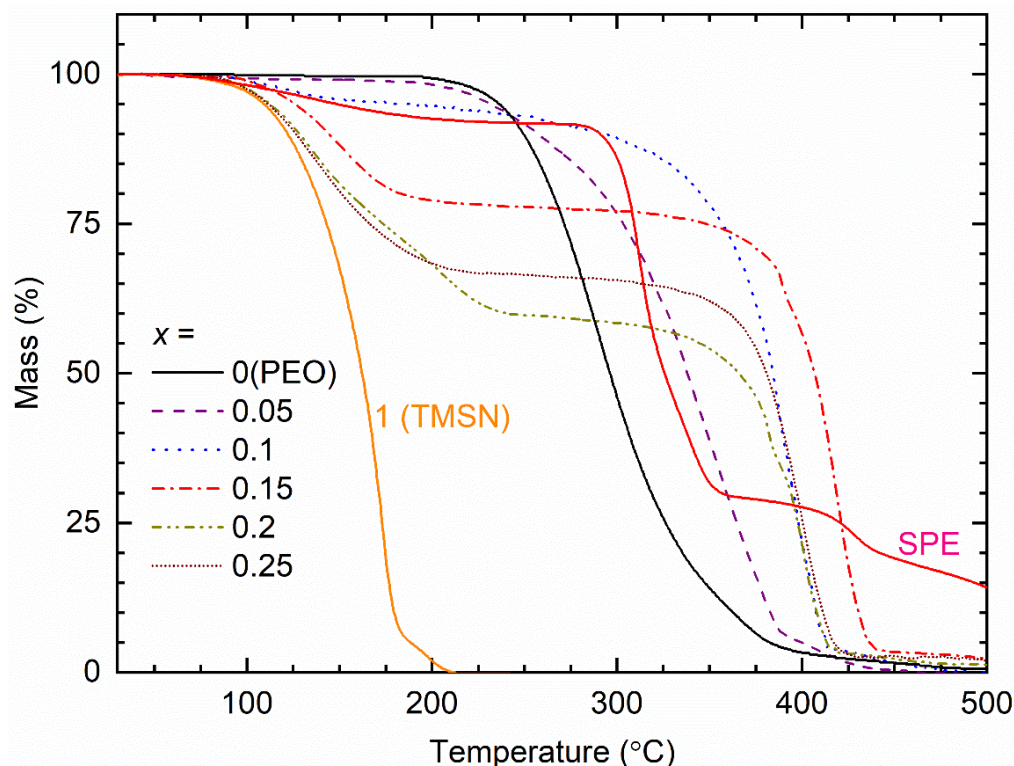


Figure 8. (a) Values of  $T_m$ ,  $T_{ep}$ , and  $T_{PC}$  of the [(1-x)PEO: xTMSN] blends, where  $x = 0-0.25$  mole. (b) Crystallinity ( $\chi$ ) of PEO and TMSN for the blends. For details, see the text.

Figure 9 shows TGA curves of the  $[(1-x)\text{PEO}: x\text{TMSN}]$  blends ( $x = 0-0.25$  mole) and pure TMSN ( $x = 1$  mole) for comparison. The PEO portrayed a flattened region up to  $\sim 200$  °C and a huge drop ( $\sim 95\%$ ) from 200 to 400 °C. The initial flattened region is the thermal stability of the polymer, and the drop is due to the degradation/burning out of the polymer [37–39,55]. The degradation products comprised formaldehyde, ethanol, low molecular weight poly(ethylene oxide), carbon dioxide, water, and nearly 20 saturated and unsaturated compounds in the range of one to seven carbons [55,56]. The addition of a small amount of TMSN ( $x = 0.05$  mole) unaltered the thermal stability of the blend significantly; instead, it slowed down the rate of degradation/burning out of the polymer because of the composite phenomenon [57,58]. The blends with  $x = 0.1-0.25$  mole, however, showed the following regions, (i) a plateau up to  $\sim 75$  °C, (ii) a small drop, (iii) a near plateau region, and (iv) a large drop. These steps were dependent on the value of  $x$ . As visualized, the initial drop was due to the TMSN degradation/sublimation, which is the lowest for the blend with  $x = 0.1$  mole and the highest for the blend with  $x = 0.2$  mole [37]. As mentioned earlier, the final drop was due to the thermal degradation of the PEO. It seems that the eutectic phase formation and phase separation played crucial roles in controlling the thermal property of the blends. The (PEO–TMSN) blend showed thermal stability up to  $\sim 75$  °C, which is lower than that of the (PEO–SN) blend ( $\sim 125$  °C [37]). This is due to the  $\text{CH}_3$  group that weakened the associated C–C bonding of the TMSN [55]. Figure 9 also shows the TGA curve of the SPE, which consisted of the matrix and redox salts. It exhibited the usual pattern, (i)–(iv). The initial drop is, however, less than that of the matrix because of the redox salts [37,58]. The SPE had an initial plateau region similar to that of the matrix, making the device operational up to 75 °C.



**Figure 9.** TGA curves of the  $[(1-x)\text{PEO}: x\text{TMSN}]$  blends ( $x = 0-0.25$ , and 1 mole) and SPE.

### 3.2.3. Electrical Transport Properties

Figure 10 shows  $\log \sigma - T^{-1}$  plots for the  $[(1-x)\text{PEO}: x\text{TMSN}]$  blends, where  $x = 0-0.25$  mole. This had temperature regions I and II before and after the melting temperature of the blends, respectively. The PEO ( $x = 0$  mole) exhibited a low value of  $\sigma_{25^\circ\text{C}}$  ( $1.7 \times 10^{-10} \text{ S cm}^{-1}$ ), because of the segmental motion of long polymeric chains [25–28,37]. An increase in temperature increased the  $\sigma$ -value linearly in both regions. Region II had a  $\sigma$ -

value higher than that in region I because region II is the amorphous region [25–28,37]. The linear  $\log \sigma - T^{-1}$  curve is expressed by the Arrhenius equation,  $\sigma = \sigma_0 \exp[-E_a/k_B T]$  [25–28,37]. This has notations,  $\sigma_0$  for a pre-exponential factor and  $k_B$  for the Boltzmann constant. The slope of the linear curve yielded the activation energy ( $E_a$ ) with a value of 1.44 eV in region I and 0.21 eV in region II. The blending of PEO with TMSN did not change the  $\log \sigma - T^{-1}$  pattern. However, it improved the electrical transport properties of the blends. For examples, the  $\sigma_{25^\circ\text{C}}$ -value increased to  $1 \times 10^{-9} \text{ S cm}^{-1}$  for  $x = 0.05$  mole,  $1.3 \times 10^{-9} \text{ S cm}^{-1}$  for  $x = 0.1$  mole,  $1.9 \times 10^{-9} \text{ S cm}^{-1}$  for  $x = 0.15$  mole, and  $2 \times 10^{-9} \text{ S cm}^{-1}$  for  $x = 0.25$  mole. The  $E_a$ -value reduced to 0.73 eV (region I) and 0.07 eV (region II) for  $x = 0.05$  mole, 0.84 eV (region I) and 0.14 eV (region II) for  $x = 0.1$  mole, 0.76 eV (region I) and 0.04 eV (region II) for  $x = 0.15$  mole, and 0.82 eV (region I) and 0.01 eV (region II) for  $x = 0.25$  mole. This trend is similar to that observed earlier for the PEO–SN blend [37]. As suggested by the structural and thermal studies, the improvement is due to the formation of the eutectic phase with a low PEO crystallinity. This is controlled by the phase separation phenomenon.

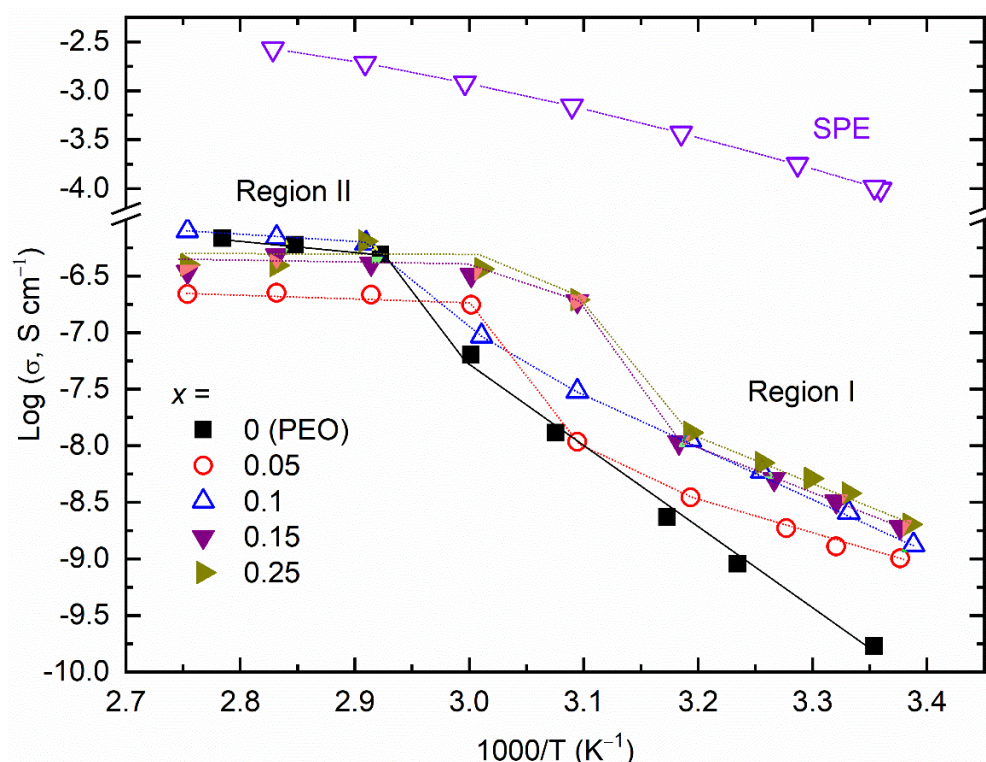


Figure 10.  $\log \sigma - T^{-1}$  plots for the [(1-x)PEO: xTMSN] blends ( $x = 0$ –0.25 mole) and SPE.

Figure 10 also exhibited the  $\log \sigma - T^{-1}$  pattern of the [0.85PEO: 0.15TMSN]–LiI–I<sub>2</sub> SPE. The SPE possessed  $\sigma_{25^\circ\text{C}}$  of  $1 \times 10^{-4} \text{ S cm}^{-1}$ , nearly five orders higher than that of the matrix. The  $\log \sigma - T^{-1}$  pattern was downward. These behaviors of the SPE are similar to those observed earlier for the (PEO–SN)–MI–I<sub>2</sub> solid redox mediators, which exhibited  $\sigma_{25^\circ\text{C}}$  of  $3 \times 10^{-4} \text{ S cm}^{-1}$  for  $M = \text{Li}$  and  $7 \times 10^{-4} \text{ S cm}^{-1}$  for  $M = \text{K}$  [38,39]. Recently, Gupta et al. [59] reported  $\sigma_{25^\circ\text{C}} \sim 7 \times 10^{-4} \text{ S cm}^{-1}$  with the downward  $\log \sigma - T^{-1}$  pattern for the solid  $\text{Co}^{2+}/\text{Co}^{3+}$  redox mediator, (PEO–SN)–LiTFSI–Co(bpy)<sub>3</sub>(TFSI)<sub>2</sub>–Co(bpy)<sub>3</sub>(TFSI)<sub>3</sub>. The downward nature revealed the supremacy of the amorphous regions over the semi-random motion of short polymer chains for ion transport. This finding is similar to the FT-IR spectroscopy, XRD, and DSC results. The amorphous domains-dominated ion transport phenomenon follows the Vogel–Tamman–Fulcher empirical relation:  $\sigma = \sigma_0 T^{-\frac{1}{2}} \exp[-B/k_B(T - T_0)]$ , where  $T_0$  is the temperature at which the free volume vanishes [25–28,38,39,59]. The linear curve of  $\log \sigma T^{\frac{1}{2}}$  vs.  $(T - T_0)^{-1}$  plot results in the pseudo-activation energy ( $B$ ), which is 0.083 eV, similar to those observed for the (PEO–SN) blend-based solid redox mediators [38,39,59]. This value is less than 0.3 eV, a requirement for the device application [57].

#### 4. Conclusions

Being members of plastic crystals, structural and thermal properties of TMSN and SN were compared. TMSN has four methyl groups by replacing the hydrogen atom of the SN. This replacement resulted in a higher molecular weight, thereby the higher  $T_m$  and  $T_{PC}$  values. The TMSN had five reflection peaks with lower  $2\theta$ -values instead of two peaks of the SN in the XRD pattern. This also led to a redshift in several vibrational modes and the crystal field splitting phenomenon. A partial replacement of PEO by TMSN with 0.1 to 0.15 mole was noted as useful in terms of the eutectic phase formation with a low PEO crystallinity, a low phase separation, thermal stability up to 75 °C, an order higher  $\sigma_{25^\circ\text{C}}$ -value, and nearly half of the activation energy of the PEO. A solid polymer electrolyte, utilizing [0.85PEO: 0.15TMSN] blend as a matrix and  $\text{LiI}-\text{I}_2$  as redox salts, exhibited  $\sigma_{25^\circ\text{C}}$  of  $\sim 1 \times 10^{-4} \text{ S cm}^{-1}$  with a pseudo-activation energy of  $\sim 0.08 \text{ eV}$  because of the formation of the amorphous phase.

**Author Contributions:** Conceptualization, R.K.G. and I.B.; methodology, R.K.G. and I.B.; formal analysis, R.K.G. and H.S.; investigation, R.K.G., H.S. and A.I.; writing—original draft preparation, R.K.G.; writing—review and editing, R.K.G., I.B. and A.S.A.; supervision, R.K.G.; project administration, R.K.G.; funding acquisition, R.K.G., I.B. and A.S.A. All authors have read and agreed to the published version of the manuscript.

**Funding:** This work was funded by the National Plan for Science, Technology, and Innovation (MAARIFAH), King Abdulaziz City for Science and Technology, Kingdom of Saudi Arabia, award number (13-ENE886-02).

**Data Availability Statement:** Data are available upon request from the corresponding author.

**Conflicts of Interest:** The authors declare no conflict of interest.

#### References

1. Hagfeldt, A.; Boschloo, G.; Sun, L.C.; Kloo, L.; Pettersson, H. Dye-sensitized solar cells. *Chem. Rev.* **2010**, *110*, 6595–6663. [[CrossRef](#)] [[PubMed](#)]
2. Ye, M.D.; Wen, X.R.; Wang, M.Y.; Iocozzia, J.; Zhang, N.; Lin, C.J.; Lin, Z.Q. Recent advances in dye-sensitized solar cells: From photoanodes, sensitizers and electrolytes to counter electrodes. *Mater. Today* **2015**, *18*, 155–162. [[CrossRef](#)]
3. Gong, J.W.; Sumathy, K.; Qiao, Q.Q.; Zhou, Z.P. Review on dye-sensitized solar cells (DSSCs): Advanced techniques and research trends. *Renew. Sustain. Energy Rev.* **2017**, *68*, 234–246. [[CrossRef](#)]
4. Rondan-Gomez, V.; De Los Santos, I.; Seuret-Jimenez, D.; Ayala-Mato, F.; Zamudio-Lara, A.; Robles-Bonilla, T.; Courel, M. Recent advances in dye-sensitized solar cells. *Appl. Phys. A Mater. Sci. Process.* **2019**, *125*, 836. [[CrossRef](#)]
5. Kokkonen, M.; Talebi, P.; Zhou, J.; Asgari, S.; Soomro, S.A.; Elsehrawy, F.; Halme, J.; Ahmad, S.; Hagfeldt, A.; Hashmi, S.G. Advanced research trends in dye-sensitized solar cells. *J. Mater. Chem. A* **2021**, *9*, 10527–10545. [[CrossRef](#)] [[PubMed](#)]
6. Green, M.A.; Dunlop, E.D.; Hohl-Ebinger, J.; Yoshita, M.; Kopidakis, N.; Hao, X. Solar cell efficiency tables (version 59). *Prog. Photovolt. Res. Appl.* **2022**, *30*, 3–12. [[CrossRef](#)]
7. Mathew, S.; Yella, A.; Gao, P.; Humphry-Baker, R.; Curchod, B.F.E.; Ashari-Astani, N.; Tavernelli, I.; Rothlisberger, U.; Nazeeruddin, M.K.; Gratzel, M. Dye-sensitized solar cells with 13% efficiency achieved through the molecular engineering of porphyrin sensitizers. *Nat. Chem.* **2014**, *6*, 242–247. [[CrossRef](#)]
8. Zhang, L.; Yang, X.C.; Wang, W.H.; Gurzadyan, G.G.; Li, J.J.; Li, X.X.; An, J.C.; Yu, Z.; Wang, H.X.; Cai, B.; et al. 13.6% efficient organic dye-sensitized solar cells by minimizing energy losses of the excited state. *ACS Energy Lett.* **2019**, *4*, 943–951. [[CrossRef](#)]
9. Kakiage, K.; Aoyama, Y.; Yano, T.; Oya, K.; Fujisawa, J.; Hanaya, M. Highly-efficient dye-sensitized solar cells with collaborative sensitization by silyl-anchor and carboxy-anchor dyes. *Chem. Commun.* **2015**, *51*, 15894–15897. [[CrossRef](#)]
10. Vlachopoulos, N.; Hagfeldt, A.; Benesperi, I.; Freitag, M.; Hashmi, G.; Jia, G.B.; Wahyuono, R.A.; Plentz, J.; Dietzek, B. New approaches in component design for dye-sensitized solar cells. *Sustain. Energy Fuels* **2021**, *5*, 367–383. [[CrossRef](#)]
11. Srivishnu, K.S.; Prasanthkumar, S.; Giribabu, L. Cu(II/I) redox couples: Potential alternatives to traditional electrolytes for dye-sensitized solar cells. *Mater. Adv.* **2021**, *2*, 1229–1247. [[CrossRef](#)]
12. Nogueira, A.F.; Longo, C.; De Paoli, M.A. Polymers in dye sensitized solar cells: Overview and perspectives. *Coord. Chem. Rev.* **2004**, *248*, 1455–1468. [[CrossRef](#)]
13. Li, B.; Wang, L.D.; Kang, B.N.; Wang, P.; Qiu, Y. Review of recent progress in solid-state dye-sensitized solar cells. *Sol. Energy Mater. Sol. Cells* **2006**, *90*, 549–573. [[CrossRef](#)]
14. Singh, P.K.; Nagarale, R.K.; Pandey, S.P.; Rhee, H.W.; Bhattacharya, B. Present status of solid state photoelectrochemical solar cells and dye sensitized solar cells using peo-based polymer electrolytes. *Adv. Nat. Sci. Nanosci. Nanotechnol.* **2011**, *2*, 023002. [[CrossRef](#)]

15. Wu, J.H.; Lan, Z.; Lin, J.M.; Huang, M.L.; Huang, Y.F.; Fan, L.Q.; Luo, G.G. Electrolytes in dye-sensitized solar cells. *Chem. Rev.* **2015**, *115*, 2136–2173. [[CrossRef](#)]
16. Su'ait, M.S.; Rahman, M.Y.A.; Ahmad, A. Review on polymer electrolyte in dye-sensitized solar cells (DSSCs). *Sol. Energy* **2015**, *115*, 452–470. [[CrossRef](#)]
17. Singh, R.; Polu, A.R.; Bhattacharya, B.; Rhee, H.W.; Varlikli, C.; Singh, P.K. Perspectives for solid biopolymer electrolytes in dye sensitized solar cell and battery application. *Renew. Sustain. Energy Rev.* **2016**, *65*, 1098–1117. [[CrossRef](#)]
18. Mehmood, U.; Al-Ahmed, A.; Al-Sulaiman, F.A.; Malik, M.I.; Shehzad, F.; Khan, A.U.H. Effect of temperature on the photovoltaic performance and stability of solid-state dye-sensitized solar cells: A review. *Renew. Sustain. Energy Rev.* **2017**, *79*, 946–959. [[CrossRef](#)]
19. Venkatesan, S.; Lee, Y.L. Nanofillers in the electrolytes of dye-sensitized solar cells—A short review. *Coord. Chem. Rev.* **2017**, *353*, 58–112. [[CrossRef](#)]
20. Iftikhar, H.; Sonai, G.G.; Hashmi, S.G.; Nogueira, A.F.; Lund, P.D. Progress on electrolytes development in dye-sensitized solar cells. *Materials* **2019**, *12*, 1998. [[CrossRef](#)]
21. Hasan, M.M.; Islam, M.D.; Rashid, T.U. Biopolymer-based electrolytes for dye-sensitized solar cells: A critical review. *Energy Fuels* **2020**, *34*, 15634–15671. [[CrossRef](#)]
22. Wang, N.; Hu, J.J.; Gao, L.G.; Ma, T.L. Current progress in solid-state electrolytes for dye-sensitized solar cells: A mini-review. *J. Electron. Mater.* **2020**, *49*, 7085–7097. [[CrossRef](#)]
23. Abu Talip, R.A.; Yahya, W.Z.N.; Bustam, M.A. Ionic liquids roles and perspectives in electrolyte for dye-sensitized solar cells. *Sustainability* **2020**, *12*, 7598. [[CrossRef](#)]
24. Teo, L.P.; Buraidah, M.H.; Arof, A.K. Polyacrylonitrile-based gel polymer electrolytes for dye-sensitized solar cells: A review. *Ionics* **2020**, *26*, 4215–4238. [[CrossRef](#)]
25. Torell, L.M.; Schantz, S. Light scattering in polymer electrolytes. In *Polymer Electrolyte Reviews—2*; MacCallum, J.R., Vincent, C.A., Eds.; Elsevier: London, UK, 1989; p. 359.
26. Gray, F.M. *Solid Polymer Electrolytes: Fundamentals and Technological Applications*; Wiley-VCH: Weinheim, Germany, 1991.
27. Sequeira, C.A.C.; Santos, D.M.F. *Polymer Electrolytes: Fundamentals and Applications*, 1st ed.; Woodhead Publishing: Cambridge, UK, 2010; pp. 1–623.
28. Ngai, K.S.; Ramesh, S.; Ramesh, K.; Juan, J.C. A review of polymer electrolytes: Fundamental, approaches and applications. *Ionics* **2016**, *22*, 1259–1279. [[CrossRef](#)]
29. Kang, M.S.; Kim, J.H.; Kim, Y.J.; Won, J.; Park, N.G.; Kang, Y.S. Dye-sensitized solar cells based on composite solid polymer electrolytes. *Chem. Commun.* **2005**, *2005*, 889–891. [[CrossRef](#)]
30. Zhou, Y.F.; Xiang, W.C.; Chen, S.; Fang, S.B.; Zhou, X.W.; Zhang, J.B.; Lin, Y. Influences of poly(ether urethane) introduction on poly(ethylene oxide) based polymer electrolyte for solvent-free dye-sensitized solar cells. *Electrochim. Acta* **2009**, *54*, 6645–6650. [[CrossRef](#)]
31. Bhattacharya, B.; Lee, J.Y.; Geng, J.; Jung, H.T.; Park, J.K. Effect of cation size on solid polymer electrolyte based dye-sensitized solar cells. *Langmuir* **2009**, *25*, 3276–3281. [[CrossRef](#)]
32. Singh, P.K.; Kim, K.W.; Rhee, H.W. Electrical, optical and photoelectrochemical studies on a solid peo-polymer electrolyte doped with low viscosity ionic liquid. *Electrochem. Commun.* **2008**, *10*, 1769–1772. [[CrossRef](#)]
33. Katsaros, G.; Stergiopoulos, T.; Arabatzis, I.M.; Papadokostaki, K.G.; Falaras, P. A solvent-free composite polymer/inorganic oxide electrolyte for high efficiency solid-state dye-sensitized solar cells. *J. Photochem. Photobiol. A Chem.* **2002**, *149*, 191–198. [[CrossRef](#)]
34. Stergiopoulos, T.; Arabatzis, I.M.; Katsaros, G.; Falaras, P. Binary polyethylene oxide/titania solid-state redox electrolyte for highly efficient nanocrystalline TiO<sub>2</sub> photoelectrochemical cells. *Nano Lett.* **2002**, *2*, 1259–1261. [[CrossRef](#)]
35. Han, H.W.; Liu, W.; Zhang, J.; Zhao, X.Z. A hybrid poly(ethylene oxide)/poly(vinylidene fluoride)/TiO<sub>2</sub> nanoparticle solid-state redox electrolyte for dye-sensitized nanocrystalline solar cells. *Adv. Funct. Mater.* **2005**, *15*, 1940–1944. [[CrossRef](#)]
36. Zhou, Y.F.; Xiang, W.C.; Chen, S.; Fang, S.B.; Zhou, X.W.; Zhang, J.B.; Lin, Y. Improvements of photocurrent by using modified sio<sub>2</sub> in the poly(ether urethane)/poly(ethylene oxide) polymer electrolyte for all-solid-state dye-sensitized solar cells. *Chem. Commun.* **2009**, *2009*, 3895–3897. [[CrossRef](#)] [[PubMed](#)]
37. Gupta, R.K.; Kim, H.M.; Rhee, H.W. Poly(ethylene oxide): Succinonitrile—A polymeric matrix for fast-ion conducting redox-couple solid electrolytes. *J. Phys. D Appl. Phys.* **2011**, *44*, 205106. [[CrossRef](#)]
38. Gupta, R.K.; Rhee, H.W. Effect of succinonitrile on electrical, structural, optical, and thermal properties of poly(ethylene oxide)-succinonitrile /LiI-I<sub>2</sub> redox-couple solid polymer electrolyte. *Electrochim. Acta* **2012**, *76*, 159–164. [[CrossRef](#)]
39. Gupta, R.K.; Rhee, H.W. Plasticizing effect of K<sup>+</sup> ions and succinonitrile on electrical conductivity of poly(ethylene oxide)-succinonitrile /KI-I<sub>2</sub> redox-couple solid polymer electrolyte. *J. Phys. Chem. B* **2013**, *117*, 7465–7471. [[CrossRef](#)] [[PubMed](#)]
40. Gupta, R.K.; Rhee, H.W.; Bedja, I.; AlHaza, A.N.; Khan, A. Effect of laponite@nanoclay dispersion on electrical, structural, and photovoltaic properties of dispersed poly(ethylene oxide)-succinonitrile -LiI-I<sub>2</sub> solid polymer electrolyte. *J. Power Sources* **2021**, *490*, 229509. [[CrossRef](#)]
41. Timmermans, J. Plastic crystals: A historical review. *J. Phys. Chem. Solids* **1961**, *18*, 1–8. [[CrossRef](#)]
42. Cardini, G.; Righini, R.; Califano, S. Computer-simulation of the dynamics of the plastic phase of succinonitrile. *J. Chem. Phys.* **1991**, *95*, 679–685. [[CrossRef](#)]

43. Long, S.; MacFarlane, D.R.; Forsyth, M. Ionic conduction in doped succinonitrile. *Solid State Ion.* **2004**, *175*, 733–738. [[CrossRef](#)]
44. Alarco, P.J.; Abu-Lebdeh, Y.; Abouimrane, A.; Armand, M. The plastic-crystalline phase of succinonitrile as a universal matrix for solid-state ionic conductors. *Nat. Mater.* **2004**, *3*, 476–481. [[CrossRef](#)]
45. Lide, D.R. *Crc Handbook of Chemistry and Physics*, 89th ed.; CRC Press/Taylor and Francis: Boca Raton, FL, USA, 2009.
46. Gupta, R.K.; Bedja, I. Cationic effect on dye-sensitized solar cell properties using electrochemical impedance and transient absorption spectroscopy techniques. *J. Phys. D Appl. Phys.* **2017**, *50*, 245501. [[CrossRef](#)]
47. Gupta, R.K.; Shaikh, H.; Imran, A.; Bedja, I.; Aldwayyan, A.S. Tetramethyl succinonitrile as a solid plasticizer in a poly(ethylene oxide)<sub>8</sub>-LiI-I<sub>2</sub> solid polymer electrolyte. *Macromol. Rapid Commun.* **2022**, *43*, e2100764. [[CrossRef](#)]
48. Murrill, E.; Breed, L.W. *Space Thermal Control by Use of Solid/Solid-Phase Change Materials*, 1st ed.; National Aeronautics and Space Administration: Marshall Space Flight Center: Huntsville, AL, USA, 1969; p. 1.
49. Fengler, O.I.; Ruoff, A. Vibrational spectra of succinonitrile and its 1,4-c-13(2) -, 2,2,3,3-h-2(4)—And 1,4-c-13(2)-2,2,3,3-h-2(4) -isotopomers and a force field of succinonitrile. *Spectrochim. Acta Part A Mol. Biomol. Spectrosc.* **2001**, *57*, 105–117. [[CrossRef](#)]
50. Colthup, N.B.; Daly, L.H.; Wiberley, S.E. *Introduction to Infrared and Raman Spectroscopy*, 3rd ed.; Academic Press: San Diego, CA, USA, 1990.
51. Fan, L.Z.; Hu, Y.S.; Bhattacharyya, A.J.; Maier, J. Succinonitrile as a versatile additive for polymer electrolytes. *Adv. Funct. Mater.* **2007**, *17*, 2800–2807. [[CrossRef](#)]
52. Yoshihara, T.; Tadokoro, H.; Murahashi, S. Normal vibrations of the polymer molecules of helical conformation. Iv. Polyethylene oxide and polyethylene-d4 oxide. *J. Chem. Phys.* **1964**, *41*, 2902–2911. [[CrossRef](#)]
53. Castiglioni, C. Theory of vibrational spectroscopy of polymers. In *Vibrational Spectroscopy of Polymers: Principles and Practice*; Everall, N.J., Chalmers, J.M., Griffiths, P.R., Eds.; John Wiley & Sons: Chichester, UK, 2007.
54. Whitfield, P.; Mitchell, L. *Principles and Applications of Powder Diffraction*, 1st ed.; Clearfield, A., Reibenspies, J.H., Bhuvanesh, N., Eds.; Wiley-Blackwell: Hoboken, NJ, USA, 2008; p. 226.
55. Madorsicy, S.L.; Straus, S. Thermal degradation of polyethylene oxide and polypropylene oxide. *J. Polym. Sci.* **1959**, *36*, 183–194. [[CrossRef](#)]
56. Voorhees, K.J.; Baugh, S.F.; Stevenson, D.N. An investigation of the thermal degradation of poly(ethylene glycol). *J. Anal. Appl. Pyrolysis* **1994**, *30*, 47–57. [[CrossRef](#)]
57. Agrawal, R.C.; Gupta, R.K. Superionic solids: Composite electrolyte phase—An overview. *J. Mater. Sci.* **1999**, *34*, 1131–1162. [[CrossRef](#)]
58. Denney, J.; Huang, H. Thermal decomposition characteristics of peo/libf4/lagp composite electrolytes. *J. Compos. Sci.* **2022**, *6*, 117. [[CrossRef](#)]
59. Gupta, R.K.; Shaikh, H.; Imran, A.; Bedja, I.; Ajaj, A.F.; Aldwayyan, A.S. Electrical transport, structural, optical and thermal properties of [(1-x)succinonitrile: Xpeo]-LiTFSI-Co(bpy)<sub>3</sub>(TFSI)<sub>2</sub>-Co(bpy)<sub>3</sub>(TFSI)<sub>3</sub> solid redox mediators. *Polymers* **2022**, *14*, 1870. [[CrossRef](#)] [[PubMed](#)]